Insights into the Chemistry of New Particle Formation and Growth Events in Pittsburgh Based on Aerosol Mass Spectrometry

QI ZHANG,[†] CHARLES O. STANIER,[‡] MANJULA R. CANAGARATNA,[§] JOHN T. JAYNE,[§] DOUGLAS R. WORSNOP,[§] SPYROS N. PANDIS,[‡] AND JOSE L. JIMENEZ*,[†,||]

Cooperative Institute for Research in Environmental Sciences (CIRES) and Department of Chemistry and Biochemistry, University of Colorado, Boulder, Colorado 80309-0216, Department of Chemical Engineering, Carnegie Mellon University, Pittsburgh, Pennsylvania 15213-3890, and Aerodyne Research Inc., Billerica, Massachusetts 01821-3976

New particle formation and growth events have been observed in several urban areas and are of concern due to their potential negative effects on human health. The main purpose of this study was to investigate the chemistry of ultrafine particles during the growth phase of the frequently observed nucleation events in Pittsburgh (~100 events per year) and therefore infer the mechanisms of new particle growth in the urban troposphere. An Aerodyne aerosol mass spectrometer (AMS) and two SMPS systems were deployed at the U.S. EPA Pittsburgh Supersite during September 2002. Significant nucleation events were observed in 3 out of the 16 days of this deployment, including one of the 10 strongest nucleation events observed in Pittsburgh over a period of 15 months. These events appear to be representative of the climatology of new particle formation and growth in the Pittsburgh region. Distinctive growth of sulfate, ammonium, organics, and nitrate in the ultrafine mode (33−60 nm in a vacuum aerodynamic diameter or ~18−33 nm in physical diameter) was observed during each of these three events, with sulfate always being the first (and the fastest) species to increase. Ultrafine ammonium usually increased 10−40 min later than sulfate, causing the ultrafine mode particles to be more acidic during the initial stages of the nucleation events. Significant increase of ultrafine organics often happened after 11:00 a.m., when photochemistry is more intense. This observation coupled with a parallel increase of ultrafine *m/z* 44, a mass fragment generally representative of oxygenated organic compounds, indicates that secondary organic species contribute significantly to the growth of particles at a relatively later time of the event. Among all these four species, nitrate was always a minor component of the ultrafine particles and contributed the least to the new particle growth.

* Corresponding author telephone: (303)492-3557; fax: (303)492-1149; e-mail: jose.jimenez@colorado.edu.

[†] CIRES, University of Colorado.

[‡] Carnegie Mellon University.

[§] Aerodyne Research Inc.

[||] Department of Chemistry and Biochemistry, University of Colorado.

1. Introduction

New particle formation and growth events have been observed in many locations including forested (*2*, *3*), coastal (*4*−*6*), rural/remote (*7*−*11*), arctic (*12*, *13*), and urban (*1*, *7*, *14*−*19*) areas. These events are one of the major sources of ultrafine particles in both clean and polluted atmospheres and an important mechanism for sustaining the ambient aerosol population. Given the increased toxicity of ultrafine particles (*20*) and the role of ultrafine particles in particle-related premature deaths and morbidity (*21*−*24*), the abundance of these particles after nucleation is considered as a potential human health hazard. In addition, the growth of nuclei from a detectable size of a few nanometers into particles that are optically active and efficient cloud condensation nuclei has important implications for visibility and climate (*4*, *25*, *26*).

New particle formation events have been observed in Pittsburgh, PA—a polluted urban area in the Northeastern United States—during all seasons, most frequently in spring and fall (*1*). While these events are often associated with elevated SO_2 and UV radiation, and thus presumably with high rates of H_2SO_4(g) production, classical binary H_2SO_4−H_2O nucleation theory considerably underestimates the frequency and intensity of the events (*1*). For this reason, additional species such as ammonia and/or organics have been suggested to participate in nucleation and nuclei growth (*1*). To some extent, this hypothesis is supported by recent model and field studies, which suggest that ternary nucleation ($H_2SO_4 + NH_3 + H_2O$) may be an efficient and prevalent new particle formation mechanism in the troposphere (*8*, *9*, *25*, *27*, *28*) and that the growth of fresh nuclei (1−3 nm in diameter) often requires the involvement of species other than H_2SO_4 and H_2O (*25*, *29*, *30*). Nevertheless, to identify the compounds that are responsible for new particle formation and growth, it is necessary to study the chemistry and dynamics of ultrafine particles in the atmosphere with direct measurements.

The evolution of the particle number concentration and size distribution during nucleation has been characterized in a number of field studies, often with techniques such as scanning mobility particle sizers (SMPS; also known as differential mobility particle sizers or DMPS) (*1*, *31*, *32*) and ultrafine condensation particle counters (UCPC) (*4*, *11*, *31*, *33*). However, none of these techniques determine particle composition. Recently a thermal desorption chemical ionization mass spectrometer (TDCIMS) that is able to quantify the composition of nucleation mode particles has been described (*34*, *35*). This instrument has been employed to study atmospheric nucleation in Atlanta, GA, where it was found that newly formed aerosol in the 8−15 nm diameter range were composed of sulfate that is neutralized to varying degrees by ammonium (*36*).

Besides TDCIMS, the aerosol mass spectrometer (AMS) developed by Aerodyne Research Inc. (*37*, *38*) is also able to determine the composition of ultrafine particles. Despite its comparatively larger minimum-size cutoff (~30−35 nm in a vacuum aerodynamic diameter or ~20 nm in physical diameter, see section 2.3.1), the AMS is a powerful tool for studying new particle growth events in the atmosphere because of it fast time response, high sensitivity, and simultaneous measurement of the particle size distribution

10.1021/es035417u CCC: $27.50
Published on Web 00/00/0000

TABLE 1. Summary of Conditions during Nucleation Events and in Base Case Situations during September 7−22, 2002[a]

nucleation starting time[b]	event intensity	N_{tot}[c] (cm^{-3})	dN_{tot}/dt[d] ($cm^{-3}\ h^{-1}$)	N_{10}[c] (cm^{-3})	dN_{10}/dt[d] ($cm^{-3}\ h^{-1}$)	N_{30-78}[c] ($cm^{3}\ s^{-1}$)	M[e] ($\mu g\ m^{-3}$)	M_{33-60}[f] ($\mu g\ m^{-3}$)	RH (%)	T (°C)	P (Torr)	SO_2 (ppb)	NO (ppb)	CO (ppm)	UV (Wm^{-2})	CS (cm^{-2})
Nucleation Periods																
9/8/02, 10:30	Strong	1.2E+05[g]	2.4E+05	2.8E+04	1.2E+05	2.3E+04	20.2	0.70	35	28	740	62	3.4	0.60	28.0	1.0E−02
9/9/02, 9:45	Moderate	4.1E+04[g]	1.2E+04	1.6E+04	1.4E+04	8.6E+03	11.5	0.53	36	27	738	6.1	11.5	0.76	23.5	3.8E−03
9/12/02, 8:15	Strong	1.0E+05	2.1E+05	6.9E+04	1.9E+05	5.5E+03	6.0	0.33	53	17	737	33	11	0.51	17.0	7.3E−03
Statistics for Nucleation Periods																
average		8.9E+04	1.5E+05	3.8E+04	1.1E+05	1.2E+04	12.6	0.52	41	24	738	33	8.8	0.63	22.8	7.0E−03
1σ		4.3E+04	1.2E+05	2.8E+04	8.6E+04	9.5E+03	7.14	0.18	10	6	2	28	4.7	0.13	5.6	3.1E−03
median		1.0E+05	2.1E+05	2.8E+04	1.2E+05	8.6E+03	11.5	0.53	36	27	738	33	11.5	0.60	23.5	7.3E−03
min		4.1E+04	1.2E+04	1.6E+04	1.4E+04	5.5E+03	6.01	0.33	35	17	737	6.1	3.4	0.51	17.0	3.8E−03
max		1.2E+05	2.4E+05	6.9E+04	1.9E+05	2.3E+04	20.2	0.70	53	28	740	62	12	0.76	28.0	1.0E−02
Statistics for Base Case Situation[a]																
average		2.5E+04		1.0E+04		5.6E+03	14.3	0.22	69	22	735	6.0	11	0.73	12.6	9.0E−03
1σ		1.1E+04		9.4E+03		4.2E+03	10.2	0.25	16	4	2	5.6	19	0.24	8.0	5.9E−03
median		2.3E+04		6.9E+03		3.5E+03	12.9	0.15	68	22	735	4.0	3.8	0.69	10.4	7.9E−03
min		6.9E+03		5.2E+02		5.9E+02	0.76	0.57	29	15	730	0.5	1.9	0.40	1.8	1.2E−03
max		9.1E+04		7.4E+04		1.8E+04	60.9	1.26	96	31	738	36	133	1.66	30.1	3.1E−02

[a] The reported variables are the average of the 2-h period from the beginning of a given nucleation event (see footnote *b*). The base case situations are the average between 8:15 a.m. and 13:00 p.m. during nonnucleation days. All times are in Eatern Standard Time. [b] Defined as the time when N_{10} shows detectable increase. [c] Particle number counts measured by the SMPS with mobility diameters indicated in the subscript. Specifically, N_{tot}: total number of particles in 3−680 nm unless flagged (see footnote *g*); N_{10}: $D_m = 3-10$ nm; N_{30-78}: $D_m = 30-78$ nm. [d] Average increase rates (calculated by a linear fit) of particle number or total mass during the time period from the starting of the nucleation to when N_{10} peaks (i.e., 10:45−11:30 a.m. on 9/8/2002; 9:45−11:15 a.m. on 9/9/2002; and 8:15−9:00 a.m. on 9/12/2002). [e] Total fine particulate mass measured by the AMS; $[M] = [SO_4^{2-}] + [NO_3^-] + [NH_4^+] +$ [organics]. [f] Total mass of ultrafine particles (i.e., $D_{va} = 33-60$ nm). [g] No particle number data available above 78 nm; therefore, N_{tot} is the sum of particle number in 3−78 nm.

for ~10−20 ion mass to charge ratios (i.e., m/z values). Indeed, the AMS has been successfully applied in a recent environmental ("smog") chamber study on new particle formation and growth (*6*, *39*).

In September 2002, an Aerodyne AMS, together with two SMPS systems, was operated at the Pittsburgh U.S. EPA Supersite as part of the Pittsburgh Air Quality Study (PAQS) (*40*). One of the main purposes of this deployment was to characterize the chemistry of particles during the growth phase of the frequently observed nucleation events in Pittsburgh. We report here (i) the temporal variations of particle size, number, and composition during the nucleation events; (ii) the dynamics of chemical species in the ultrafine particles; and (iii) the possible mechanisms responsible for the growth of ultrafine particles.

2. Experimental Methods

2.1. Sampling Time and Location. All measurements in this study were conducted on the main PAQS sampling site (40°27′ N, 79°57′ W) at Schenley Park right next to the campus of Carnegie Mellon University, which is about 6 km east of downtown Pittsburgh (*40*). The AMS operated continuously for 16 days from September 7 to September 22, 2002. The Supersite, including the SMPS systems and gas-phase and meteorology measurements, was operated far longer, almost continuously from July 2001 to October 2002 (*40*). The study described here only encompasses the AMS operation period. All reported dates and times are Eastern Standard Time (EST).

2.2. Instrumentation and Measurements.

2.2.1. Measurements of Particle Composition. Mass concentrations and size distributions of submicron nonrefractory sulfate, nitrate, ammonium, and organics were measured with the AMS. Detailed descriptions of the Aerodyne AMS can be found elsewhere (*37*, *38*, *41*). Specific information on the AMS operation and data analysis during this study is presented in another paper (*42*), and only the main points are given here. Two new techniques were applied to improve the determination of the NH_4^+ size distribution for ultrafine particles. These involved (a) removing the interference of gaseous O^+ (m/z 16) signal on the size distributions of the NH_2^+ fragment of ammonium below 100 nm (*42*) and (b) correcting the NH_4^+ size distributions for the faster ion flight from ionizer to detector by ~60 μs as compared to sulfate (*42*). Details of the new techniques and of the standard technique for determining NH_4^+ mass concentrations from AMS data are presented in two other publications (*42*, *43*).

The averaging time for the AMS measurements was 10 min initially and 5 min after 9:40 a.m., September 12, 2002. The AMS has nearly 100% transmission efficiency for particles in the size range of 60−600 nm vacuum aerodynamic diameters (D_{va}) and partial transmission up to 1500 nm (*37*). On the basis of our size calibrations, we estimated that the lower transmission limit of the AMS was ~33 nm (D_{va}) with an uncertainty of up to 7 nm (*42*). No attempt was made to correct the measured size distributions for partial transmission of larger and smaller particles. While this may lead to an underestimation of the growth rate of ultrafine species, it does not affect our ability of identifying the species that are responsible for the growth.

2.2.2. Measurements of Particle Number and Size Distributions. Two scanning mobility particle sizers (SMPS), a TSI 3936N25 nano-SMPS (3−83 nm) and a TSI 3936L10 SMPS (10−680 nm), were operated to measure particle number concentration as a function of mobility diameter (D_m) (*1*). The SMPS systems sampled alternatively between dry (<30%) and humid (at ambient relatively humidity) modes but only the dry-mode data are reported here. Each SMPS size distribution used here is the average of two upscans (5 min each) onto a 15-min time interval. A single size distribution from 3 to 680 nm D_m was formed by merging data from these two SMPS systems and using data from the nano-SMPS up to 30 nm. No multipliers are used to enforce continuity of the size distribution.

2.2.3. Measurement of Gaseous Pollutants and Meteorology. Data on concentrations of major gaseous pollutants (SO_2, O_3, CO, NO, and NO_x), UV radiation, and other meteorological parameters were collected at a time resolution of 10 min during this study. Detailed information on these measurements is available elsewhere (*40*).

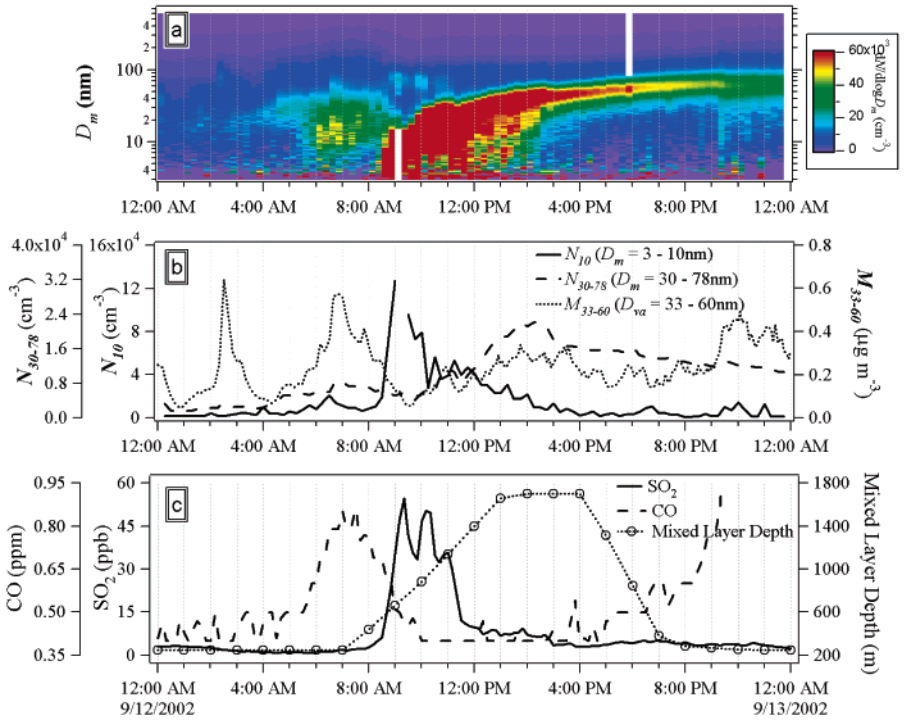

FIGURE 1. Change of (a) particle size distribution; (b) number concentration and total mass loading; and (c) SO_2, CO, and mixing layer depth as a function of time on September 12, 2002, a day with a well-defined and intense nucleation event. Mixing layer depth was calculated with the HYSPLIT4 trajectory model using EDAS wind field data.

2.3. Data Analysis.

2.3.1. Terminology. Mobility diameter (D_m) and vacuum aerodynamic diameter (D_{va}) are used in parallel throughout the paper with D_m denoting SMPS-measured sizes and D_{va} AMS sizes. Note that D_{va} (the aerodynamic diameter of particles measured in the free-molecular regime) differs from the classical aerodynamic diameter (D_{ca}; or aerodynamic diameter of particles in the continuum regime) in that (i) D_{va} is proportional to particle material density instead of the square root of the density and (ii) D_{va} and D_{ca} relate differently to the dynamic shape factor (χ) (*39*, *44*). D_m is also dependent on χ but not on particle material density. As a result, the ratio of D_{va} to D_m is a function of size, composition, shape, and relative humidity for ambient particles. However, the D_{va} to D_m ratio simplifies to particle density for spherical particles, for which $\chi = 1$. The average density for the bulk Pittsburgh particles (usually dominated by the accumulation mode) was estimated to be roughly 1.5 during this study, based on the average particle composition (~70% ammonium, sulfate, and nitrate and ~30% organics) in Pittsburgh (*42*).

Because the new particles formed during the nucleation events in Pittsburgh appear to be mainly composed of sulfuric acid neutralized to a varying degree by ammonium and likely containing some water (due to the high hygroscopicity of H_2SO_4) by the time they are first detected by the AMS, we assume that those particles are spheres with a density of ~1.8 g/cm^3. In this way, we estimate that the smallest particles (i.e., D_{va} = 33 nm) detectable by the AMS in these events have a physical diameter of about 18 nm and contain ~200 times more mass than a 3-nm nucleus. Because of this limitation, we can directly address the question of which species contribute to the growth of new particles but not of which species formed the initial 1−3 nm nuclei. From this point of view, the AMS is complementary to the TDCIMS instrument for the study of new particle formation and growth (*34*, *35*), since the later instrument can analyze smaller particles but of only one size and composition at a time.

In this paper, the modes of the observed particle size distribution are named according to the following convention: "nucleation mode" (D_m = 3−10 nm), "ultrafine" or "Aitken mode" (D_m = 10−100 nm), and "accumulation mode" (D_m = 100−1000 nm) (*33*). Number concentrations of particles in a given size range (integrated from dN/dlogD_m) were denoted as N with their D_m range as subscripts. Specifically, N_{10} stands for the number concentration of nucleation mode particles from 3 nm (the lower detection limit of the SMPS system) to 10 nm; N_{30-78} stands for the "growth mode" from 30 to 78 nm; and N_{tot} stands for the total concentration of 3−680 nm. These size ranges are slightly different from those listed above to maximize comparability of SMPS and AMS data and also due to operational considerations for the SMPS.

By the same convention, $SO_4^{2-}{}_{33-60}$, $NH_4^+{}_{33-60}$, $NO_3^-{}_{33-60}$, and Org_{33-60} stand for the mass concentrations of SO_4^{2-}, NH_4^+, NO_3^-, and organics, respectively, in particles with D_{va} of 33 nm (the lower detection limit of the AMS) to 60 nm. The total mass of particles (referred to as M) is defined as the sum of these four species (e.g., $M_{33-60} = SO_4^{2-}{}_{33-60} + NH_4^+{}_{33-60} + NO_3^-{}_{33-60} + Org_{33-60}$. In addition, m/z 43_{33-60}, m/z 44_{33-60}, m/z 55_{33-60}, and m/z 57_{33-60} stand for the nitrate-equivalent mass concentrations of the organic fragments m/z 43, 44, 55, and 57, respectively, in 33−60 nm (D_{va}) particles. The nitrate-equivalent mass concentration of a given organic fragment equals the mass concentration of nitrate that would produce an ion signal of the same intensity (by summing the m/z 30 and 46 signals from nitrate) (*38*). The nitrate-equivalent mass concentration can be converted into the actual mass concentration by taking into account the ionization efficiency of the species relative to that of nitrate, its fragmentation pattern, and the collection efficiency of the particles (*38*, *42*). Detailed information on AMS quantification is described in a separate paper (*42*).

2.3.2. Characterizing Nucleation Events. Nucleation events were identified based on the evolution of the size distributions and particle number concentrations. Primary emissions of nucleation mode particles (e.g., from traffic) were screened out if the increase of N_{10} was comparatively low and correlated with increases of CO and NO (*1*), and the size distributions were broader than those typically observed

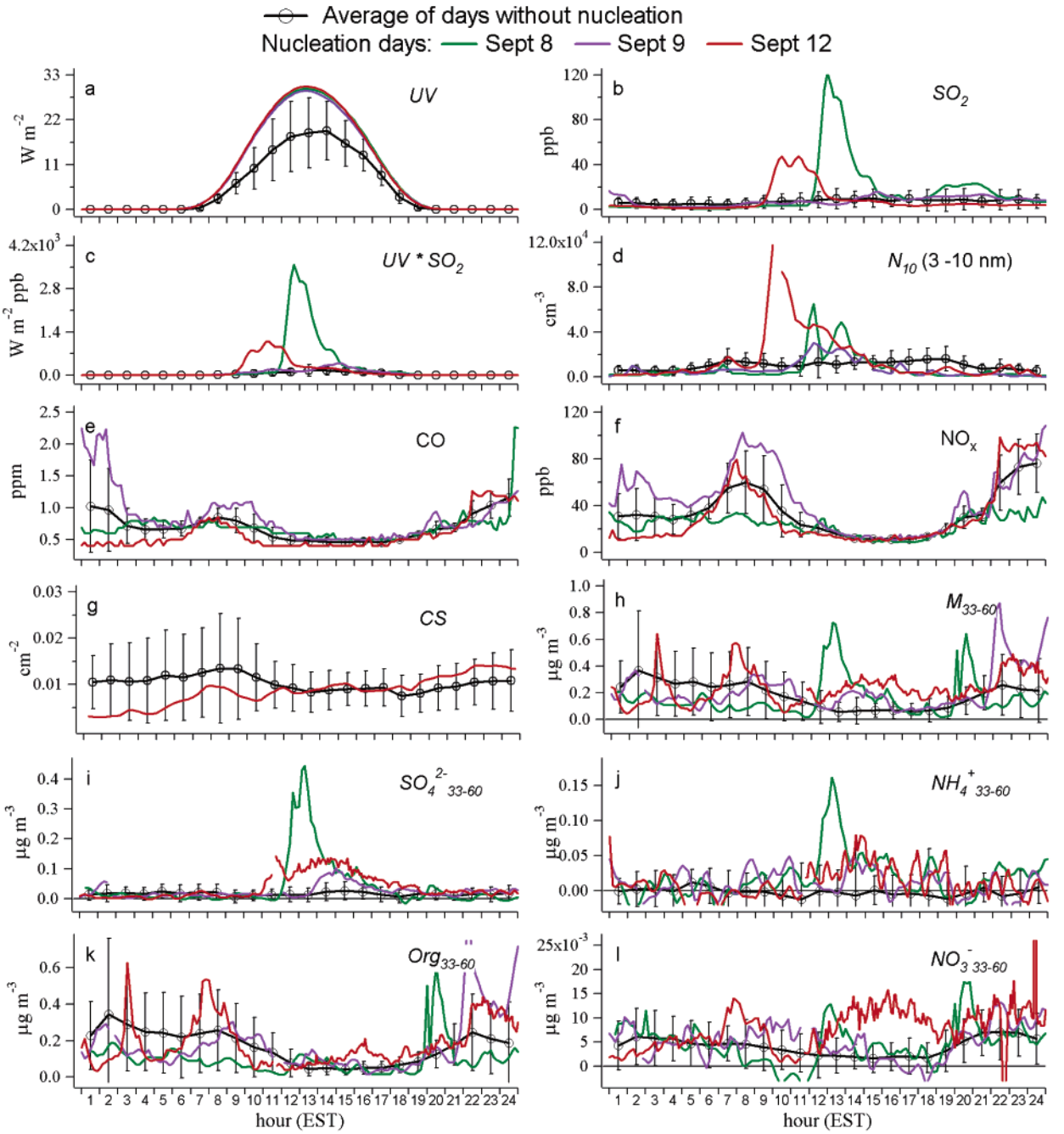

FIGURE 2. Average diurnal patterns of various parameters on days with and without nucleation events. Symbols represent average values; errors bars are one standard deviation.

during nucleation events. Once identified, nucleation events were further categorized into "weak" (dN_{10}/dt < 4000 cm^{-3} h^{-1}), "moderate" (15 000 > dN_{10}/dt > 4000 cm^{-3} s^{-1}), or "strong" (dN_{10}/dt > 15 000 cm^{-3} h^{-1}) following the classification of Stanier et al. (*1*).

2.3.3. Condensational Sink and Coagulation Time. The aerosol condensational sink (CS, in units of cm^{-2}) is a measure of the available surface area for condensation. A larger CS is less favorable for nucleation. For this study CS was integrated from D_m of 3−680 nm, the size range of the SMPS measurement, using the formulation of Pirjola et al. (*45*). Because of this incomplete integration and because our D_m values were for dry particles (see section 2.2.2), we likely underestimate the actual CS, especially for aged air masses that contain more larger particles and for periods that were relatively humid.

As an attempt to qualitatively evaluate the growth history of the ultrafine particles (i.e., D_{va} > 33 nm; the AMS measurable size range), we compared the characteristic time of coagulation to that of condensation for the nucleation mode particles. The characteristic time of coagulation was computed based on the theory of Brownian coagulation of polydisperse aerosols (*46*) using the Aerosol Calculator Program developed by Baron and Willeke (*47*).

2.3.4. Calculation of Mixed Layer Depth. Hourly values of mixed layer depths reported in this study were calculated using the Hybrid Single Particle Lagrangian Integrated Trajectory (HYSPLIT4) model and the EDAS meteorological data set available at http://www.arl.noaa.gov/ready/hysplit4.html. Note that the mixing layer depth calculated by this method can have significant uncertainties and is treated qualitatively in this study.

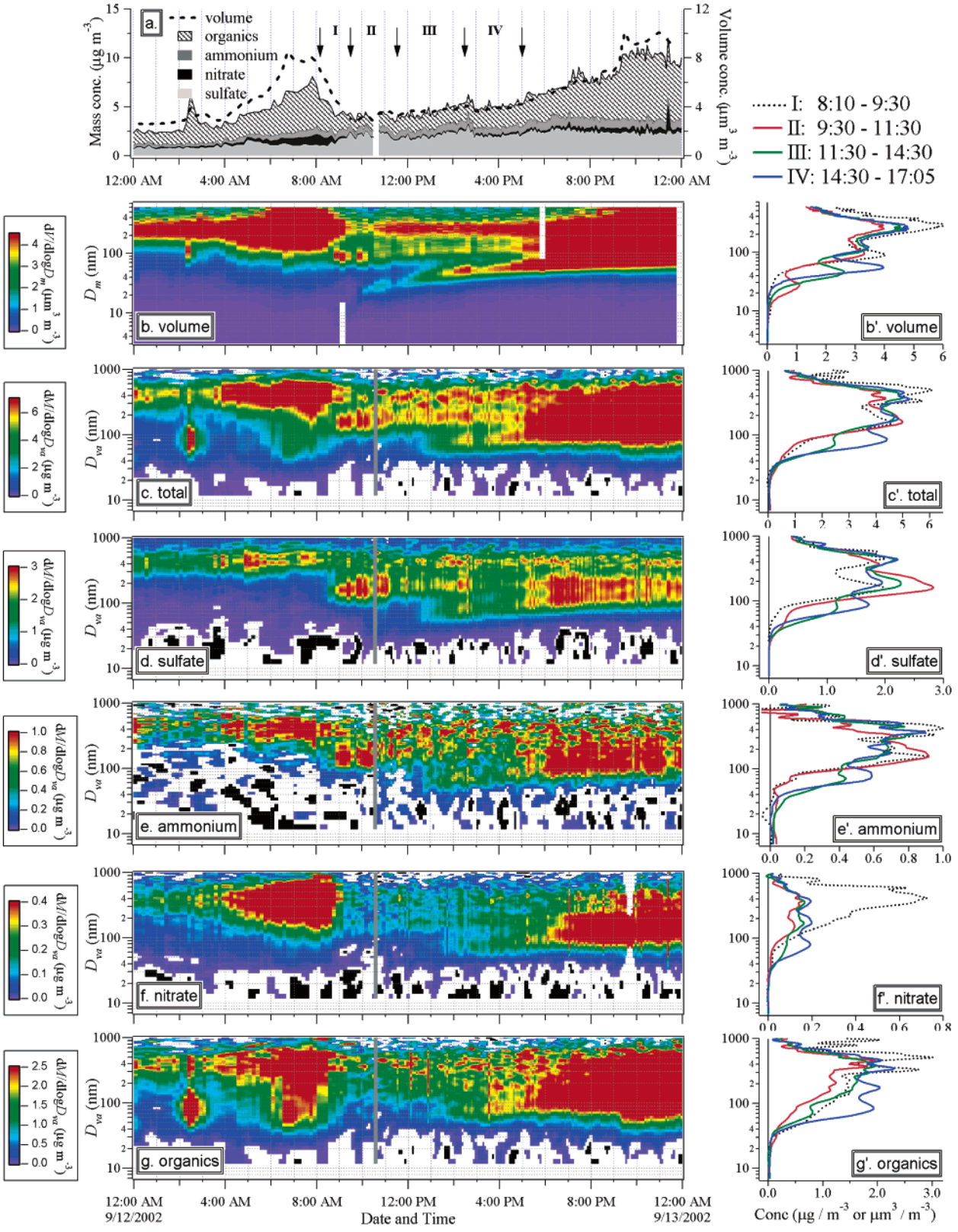

FIGURE 3. Time series of the mass concentrations of particle species and apparent volume (a) and evolutions of the size distributions for apparent volume (b), total mass concentration (c), and mass concentrations of chemical species (d−g) on September 12, 2002. The four stages (I−IV) of the nucleation and growth are marked on plot a. To the right of the corresponding image plot are the average size distributions of given parameter during these four stages (b′−g′). Particle apparent volume was calculated using SMPS number distribution data assuming spherical particles. Missing data (white areas in plot a and gray areas in plots b−g) are due to either occasional instrumental malfunction or maintenance/calibration. White areas in plots b−g are due to the omission of data points that are below the detection limit (1σ) of the AMS.

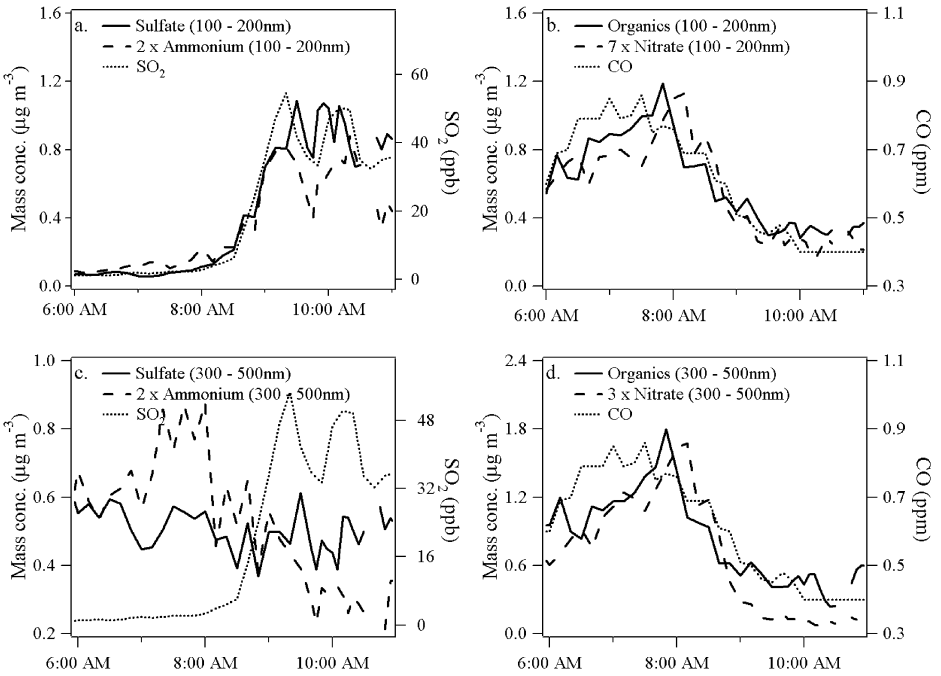

FIGURE 4. Variations in the mass concentrations of SO_4^{2-}, NH_4^+, NO_3^-, and organics in the accumulation mode (D_{va} = 300−500 nm) and the intermediate mode (D_{va} = 100−200 nm) together with those of CO and SO_2 during the initial stage of nucleation on September 12, 2002. Note that ammonium and nitrate were scaled in the graph to match sulfate and organics, respectively; see the legends in the plots for scaling factors.

3. Results and Discussion

3.1. Characteristics of the Nucleation Events.

3.1.1. General Characteristics. Three significant nucleation and particle growth events (on September 8, 9, and 12, respectively) and one weak event (on September 7) were observed during September 7−22, 2002. Although another event may have occurred on September 13 (based on the increase of the number and mass concentrations of ultrafine particles larger than 15 nm), we were not able to quantify it due to lack of information on particles below 15 nm (D_m). All events started in the morning between ~8:00 and 11:00 a.m. (Table 1). The average conditions during the initial 2-h periods of the nucleation events on September 8, 9, and 12 along with those averaged from 8:00 to 13:00 EST on nonnucleation days are summarized in Table 1. The September 7 event was not included due to large relative interference from traffic emissions. The nucleation periods are characterized by a substantial increase in the nucleation mode particles (D_m = 3−10 nm) (e.g., the average values of N_{10} ranged from 16 000 up to 69 000 cm^{-3}) as compared to an average value of ~10 000 ± 9 400 (1σ) during nonnucleation periods (Table 1). N_{tot} and N_{30-78} as well as ultrafine mass (i.e., M_{33-60}) were also significantly higher, but the average total mass loading (M; D_{va} = 33−1000 nm) was slightly lower (Table 1), indicating a smaller average aerosol size during the nucleation periods.

The events on September 8 and 12 are classified as strong, and that on September 9 was classified as moderate based on their rates of increase in N_{10} (see section 2.3.2). Figure 1 shows the evolution of particle number and size distribution on September 12, one of the 10 strongest nucleation events observed in Pittsburgh over a period of 15 months (July 1, 2001−September 30, 2002) (*1*). Sharp increase of nucleation mode particles started at ~8:10 a.m. (e.g., N10 increased by roughly a factor of 10 within ~1 h) followed by a gradual growth of the new particles (Figure 1a). Significant increase of Aitken mode particles (e.g., N_{30-78} and M_{33-60}) started roughly 1 h after that of N_{10} and lasted for ~5 h (Figure 1b). Meanwhile, synchronous increases of SO_2, decrease of CO, and rise of the calculated (HYSPLIT4) boundary layer height were observed at the start of this event (Figure 1c), indicating that these changes are likely a result of breakup of the morning inversion that mixes down SO_2-enriched but CO-depleted air from aloft and dilutes the accumulated city emissions. According to Stanier et al. (*1*), this phenomenon is fairly common in Pittsburgh during the spring and fall. The well-defined nucleation and particle growth characteristics also suggest that the event on September 12 is occurring on a regional scale (*1*).

The major traits of the development of particle number concentrations and size distributions during the other two events are generally similar to this one (Table 1) and are consistent with observations from a 15-month study of Pittsburgh nucleation (*1*). Therefore, although we only characterized three events, they appear to be representative of the climatology and the strength of nucleation events in the Pittsburgh area.

3.1.2. Diurnal Patterns. Figure 2 summarizes the 1-h average diurnal profiles of 12 parameters on days in which nucleation was not observed, together with the individual time series for the three nucleation days. In general, the diurnal profiles of nonnucleation days are comparatively flat while those of nucleation days show much more variation. In addition to higher UV radiation and elevated SO_2 (Figure 2a,b), we observed good correlation between N_{10} and the product of UV and SO_2 (a proxy for the H_2SO_4 production rate) during nucleation events (Figure 2c,d; Table 1). This observation, as well as the fact that N_{10} and UV*SO_2 rise simultaneously, suggests an essential role played by H_2SO_4 in the nucleation and early growth. Particle condensational sink before the September 12 nucleation event (those on September 8 and 9 were not calculated due to lack of SMPS data for D_m > 78 nm) was comparatively smaller than that during the same periods on nonnucleation days (Figure 2g). This observation is consistent with the finding of Stanier et al. (*1*) that low available aerosol surface favors the formation of new particles, probably through the accumulation of

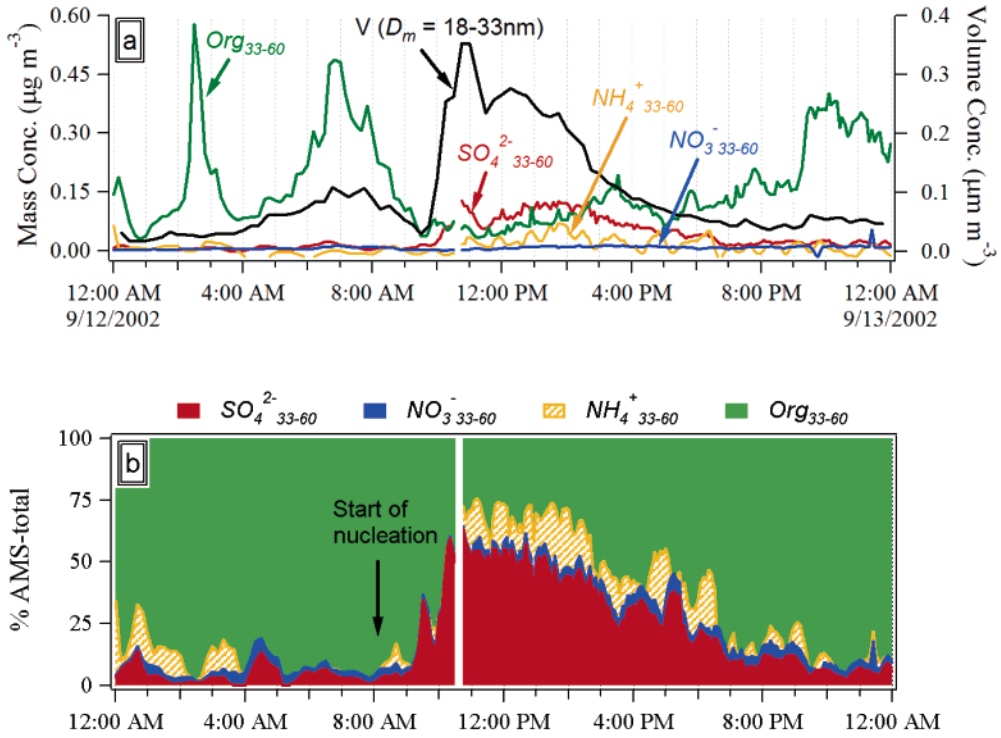

FIGURE 5. (a) Concentrations of SO_4^{2-}, NH_4^+, NO_3^-, organics, and particle volume in the 33−60 nm (D_{va}) particles on September 12, 2002. Particle volume was calculated using SMPS data in the D_m range of 18−33 nm by assuming spherical particles with density of 1.8 g cm^3. (b) Percent fraction of each species vs total (= sulfate + nitrate + ammonium + organics) in the 33−60 nm (D_{va}) particles. Missing data are due to either occasional instrumental malfunction or maintenance/calibration.

condensable species in the gas phase that can be used to nucleate and grow new particles.

The mass concentrations of sulfate, ammonium, nitrate, and organics in the 33−60 nm (D_{va}) particles all increased considerably during nucleation days, but between 20 min to 1.5 h later than the rise of N_{10} (Figure 2h−l). The lag corresponds to the time needed for the nucleation mode particles to grow into the size range detectable by the AMS. The average diurnal profile of Org_{33-60} during nonnucleation days resembles those of NO_x and CO (Figure 2e,f,k), indicating a major combustion (probably traffic) source for the small mode organics (*38*, *42*, *48*).

3.2. Evolution of Particle Chemistry during the Nucleation and Growth Event on September 12, 2002. We focus on the September 12 event because of its well-defined nucleation and growth characteristics (Figure 1) and the fact that it is one of the 10 strongest events observed in Pittsburgh in 15 months.

3.2.1. Chemistry and Dynamics of Size-Resolved Aerosol Species. Figure 3 provides an overview of the aerosol characteristics and their development on September 12, 2002. We have divided the nucleation event into four consecutive periods (I−IV) based on the dynamics of N_{10} and N_{30-78}. Stage I (8:10−9:30) corresponds to the initial nucleation period from the beginning of the rise of N_{10} to its peak; stages II (9:30−11:30) and III (11:30−14:30) represent the growth period during which N_{10} was decreasing while N_{30-78} gradually grew to its maximum; and stage IV (14:30−17:05) represents a later period of the event when both N_{10} and N_{30-78} were decreasing. Average size distributions during these four stages are plotted to the right of the corresponding image plot (Figure 3b′−g′).

As shown in Figure 3a, the aerosol mass loading increased in the early morning (likely due to rush hour traffic) and gradually decreased during stage I. This decrease coincides in time with a decrease in ambient CO concentration, an increase in SO_2, and the (modeled) rise of the mixing layer height (Figure 1c) and therefore is likely a result of dilution of the accumulated city emissions by an SO_2-enriched air mass from aloft. Particle mass concentration increased gradually after stage I but remained comparatively low for the rest of the day (Figure 3a).

The size distributions of particle apparent volume and non-refractory mass also changed considerably during this event (Figure 3b−g). The distribution of aerosol apparent volume (calculated from the corresponding SMPS number data assuming spherical particles) was dominated by a single accumulation mode centered at ∼290 nm (D_m) before nucleation and developed into a trimodal distribution soon after, with the simultaneous appearance of an intermediate mode (centered at ∼90 nm D_m) and the nucleation mode (Figure 3b,b′). Both modes grew larger in size and in volume concentration during the rest of the event. The intermediate mode, for example, grew by ∼50% from a D_m of 88 to 122 nm from stage I to stage IV, while the nucleation mode grew by a factor of 5 from 11 to 55 nm. The accumulation mode, in contrast, showed a slight increase in concentration and almost no change in size.

The size distribution of the AMS-measured aerosol mass (= sulfate + ammonium + nitrate + organics) resembles that of SMPS-measured volume (Figure 3b,c). However, because the sizing limit of the AMS (D_{va} = 33 nm) is larger than that of the SMPS (D_m = 3 nm), the smallest mode on the mass distributions appeared at a relatively later time.

The evolution of the size distributions of sulfate was very similar to those of mass and volume, except for the dynamics of the intermediate mode that emerged shortly after the nucleation (Figure 3b−d,b′−d′). The intermediate mode on particle volume distribution (D_m = 60−120 nm) declined first and then grew higher (Figure 3b′), while that of sulfate (D_{va} = ∼ 100−200 nm) did the opposite—increased significantly from stage I to stage II and gradually decreased afterward (Figure 3d′). The size distributions of ammonium, although noisier due to comparatively higher background

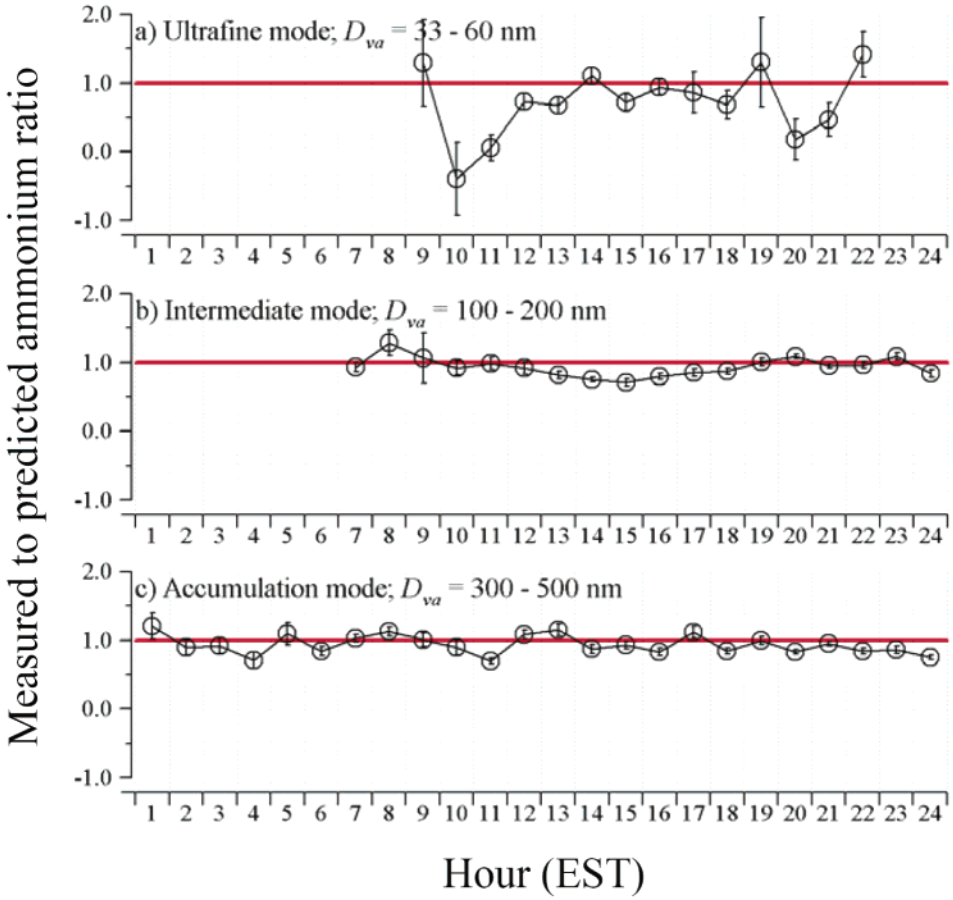

FIGURE 6. Hourly average of the mole ratio of measured NH_4^+ vs predicted NH_4^+ in three size bins of particles on September 12, 2002. Error bars are standard errors of the mean (calculated from propagation of the corresponding errors for $NH_4^+{}_{33-60}$, $SO_4^{2-}{}_{33-60}$, and $NO_3^-{}_{33-60}$ measurements and instrument noise). Note that only SO_4^{2-}, NH_4^+, and NO_3^- data that are 3 times above the AMS instrument detection limits were used to calculate the acidity values and that missing data are those below the detection limits. The predicted NH_4^+ was calculated from measured SO_4^{2-} and NO_3^- assuming full neutralization of these ions by NH_4^+. A ratio of one suggests that the aerosols are neutralized.

signal for this species in the AMS (*42*), look similar to those of sulfate on almost every aspect, even in terms of the declining of its intermediate mode from stage II to stage IV (Figure 3d,e,d′,e′). The appearance and the increase of the intermediate mode sulfate and ammonium paralleled those of SO_2 (Figure 4a), suggesting that both of them likely came from the same stable layer that capped the boundary layer before the breakup of the inversion.

The size distributions and evolution patterns of organics and nitrate are quite different from those of sulfate and ammonium, especially in the early morning before the start of the nucleation. First of all, in addition to the accumulation mode centered at D_{va} ~400 nm, organics and nitrate had an additional Aitken mode centered at ~100 nm (Figure 3f,g). The organic component of these smaller mode particles, which contained much less ammonium and sulfate, appeared to come from traffic emissions based on their time variation and their strong correlation with CO and NO_x (*42*). This mode would likely contain internally mixed soot as well; however, the AMS is not capable of detecting this material at the aerosol vaporizer temperature employed for this study (~600 °C). Increase of particulate nitrate in the early morning may be attributed to the favorable thermodynamic conditions for conversion of gaseous HNO_3 and NH_3 into NH_4NO_3 aerosol (low temperature and high RH) or to the formation of nitrate via the NO_3 radical and N_2O_5, a mechanism that is most active at night. Similar phenomenology for nitrate has been observed at other locations in the Eastern United States (*38*, *49*).

During the initial stage of the nucleation (e.g., from 8:00−9:30 a.m.), the mass concentrations of nitrate and organics in both the accumulation mode (D_{va} = 300−500 nm) and the intermediate mode (D_{va} = 100−200 nm) were gradually decreasing, together with a similar magnitude of decrease of CO (Figure 4b,d). Meanwhile, the intermediate mode sulfate and ammonium were increasing, together with a similar magnitude of increase of SO_2 (Figure 4a). Because the increase of SO_2 was likely due to mixing of SO_2-enriched air mass from aloft while the decrease of CO was due to dilution of city emissions, this intermediate mode appears to be an externally mixed combination of a major portion of $(NH_4)_2SO_4$ particles (i.e., neutralized) that came from the same air mass as SO_2 and a minor portion of preexisting urban particles that were mainly composed of organics and nitrate.

Because the size distributions of all four species were similar at D_{va} above 300 nm before the nucleation, the accumulation mode was likely aged regional aerosols consistent with an internal mixture of sulfate, ammonium, organics, and a comparatively small amount of nitrate. During the initial stage of the nucleation, all the accumulation mode species, except for sulfate, decreased in parallel with CO (Figure 4c,d) due to dilution from the air mixing down from aloft. The reason for sulfate decreasing less (Figure 4c) was probably its higher concentration in the air mass aloft and/or the larger condensation of H_2SO_4.

Despite the initial differences, during stages III and IV both nitrate and organics gradually developed into a trimodal distribution that matched those of sulfate and ammonium

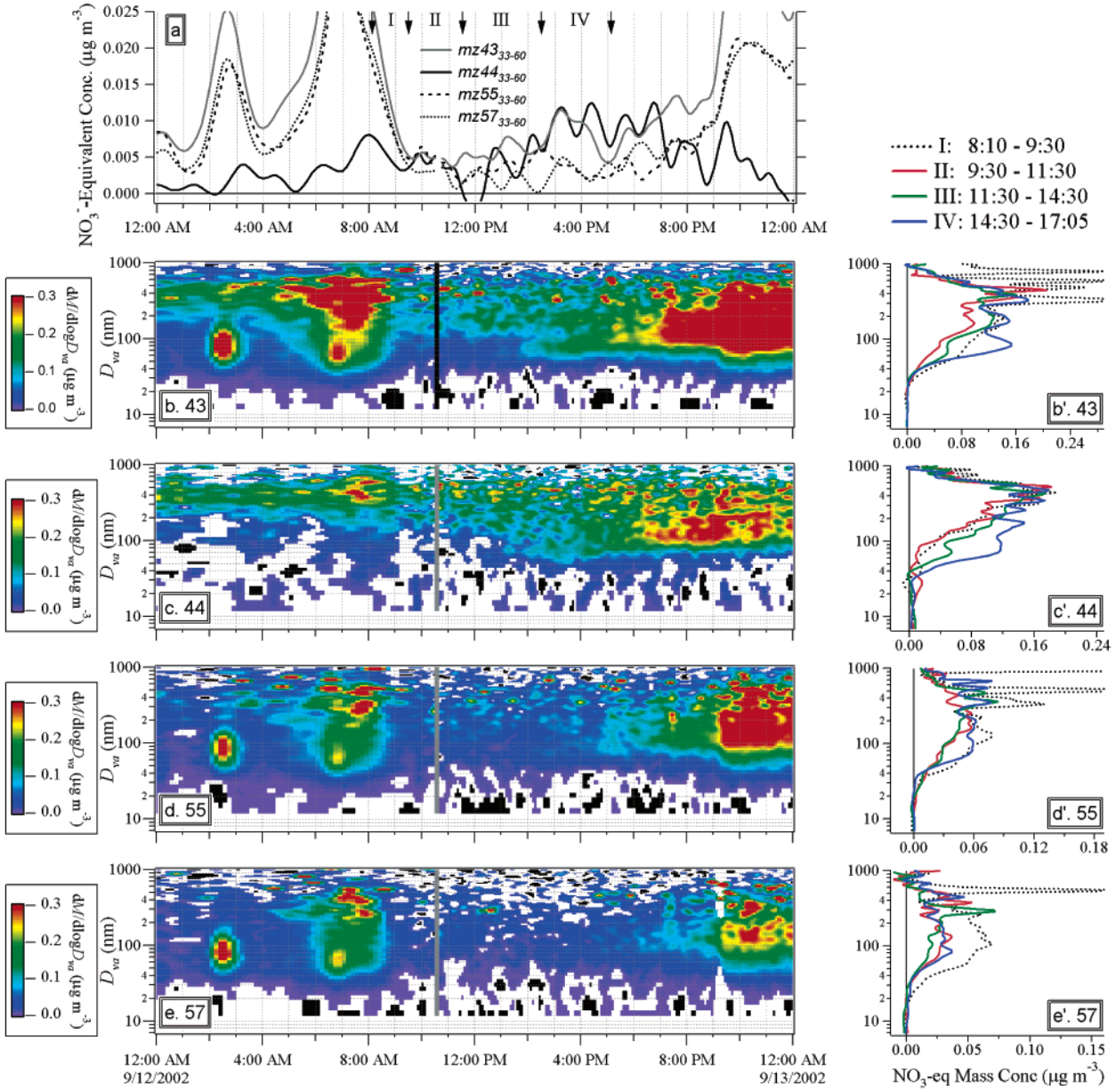

FIGURE 7. (a) Time series of the nitrate-equivalent mass concentrations of organic fragments (*m/z* 43, 44, 55, and 57) in 33−60 nm (D_{va}) particles on September 12, 2002 with the four stages of the nucleation event marked. (b−e) Evolution of the size distribution and mass concentration of these four fragments during September 12, 2002. (b′−e′). The average size distribution of a given individual component during the four stages of the nucleation event. Gray areas on plots b−e are due to either occasional instrumental malfunction or maintenance/calibration; white areas are due to the omission of data points that are below the detection limit (1σ) of the AMS. Note that NO_3^- equivalent mass concentration equals the mass concentration of nitrate that would produce a signal of same intensity, summing all of nitrate's *m/z* (see section 2.3.1).

(Figure 3c−g,c′−g′), indicating extensive condensation of gaseous precursors of nitrate and organics onto preexisting particles. This process gradually diminished the heterogeneity of the particles so that they became more internally mixed.

3.2.2. Composition and Growth of Ultrafine Particles (D_{va} = 33−60 nm). The growth of nucleation mode particles into the Aitken mode was one of the most prominent features of the nucleation event (Figures 1a and 3). The smallest mode, which was originally the nucleation mode, grew from an average D_m of 11 nm in stage I of the nucleation event gradually into 29, 46, and 55 nm subsequently across the other three stages (Figure 3b′). Due to a larger size cutoff of the AMS, this mode appeared at a later time on the mass distributions, but the growth of each species was evident. The growth appeared to proceed at different rates and probably through different mechanisms (Figure 3d−f,d′−f′).

Variations of the mass concentration of SO_4^{2-}, NH_4^+, NO_3^-, and organics in the D_{va} range 33 (the lower bound of the AMS detection) to 60 nm were thus carefully analyzed to gain insights into which species contributed to the growth, during which stage, and by what extent. Note that this size range is equivalent to D_m of 18−33 nm assuming a density of 1.8 g/cm^3 (which would be appropriate for sulfuric acid or ammonium sulfate particles) and spherical particles. It took ~1 h for the 3−10 nm (D_m) mode particles to grow into this size range during this event.

As shown in Figure 5a, the concentrations of ultrafine sulfate (i.e., $SO_4^{2-}{}_{33-60}$) were very low before the nucleation and started to increase at ~9:00 a.m. A rapid increase of

TABLE 2. Average Growth Rates of Particle Number (cm^{-3} h^{-1}) and Composition (ng m^{-3} h^{-1}) in Ultrafine Particles during Nucleation[a]

start of growth	peak of growth	dN_{30-78}/dt	dM_{33-60}/dt	$dSO_4^{2-}{}_{33-60}/dt$	$dNH_4^{+}{}_{33-60}/dt$	$dNO_3^{-}{}_{33-60}/dt$	$dOrg_{33-60}/dt$[b]
9/8/02, 11:00	9/8/02 12:10	4.7E+04	621	353	138	15	116
9/9/02, 12:00	9/9/02 14:00	1.2E+04	60	53	24	1.9	130
9/12/02, 9:30	9/12/02 11:00	5.9E+03	122	91	23	0.9	7
9/12/02, 11:30	9/12/02 14:00	5.7E+03	70	24	24	3.5	19
average		1.8E+04	218	130	52	5	68
1σ		2.0E+04	270	151	57	6.6	64
median		8.9E+03	96	72	24	2.7	67
min		5.7E+03	60	24	23	0.9	7
max		4.7E+04	621	353	138	15	130

[a] Growth rates were determined by a linear fit to the data in the time periods listed in the first two columns unless flagged. [b] Calculated for the period from when Org_{33-60} started to rise to when it peaked (i.e., 12:00−12:40 p.m.).

$SO_4^{2-}{}_{33-60}$ was observed at ~9:50 a.m., followed by the rise of $NH_4^{+}{}_{33-60}$. Very high levels of ultrafine organics were present prior to the nucleation event, probably due to traffic emissions (Figure 5a). As a result, Org_{33-60} was more sensitive to changes of the boundary layer height and thus decreased dramatically during the initial stage of the nucleation (Figures 1c and 5a).

Org_{33-60} went through a temporary rise from ~9:30 to 9:50a.m. but declined again afterward (Figure 5a). Because this rise was coincident with a small increase in CO and decreases in SO_2 and $SO_4^{2-}{}_{33-60}$, it was probably a result of elevated detection of city emissions during this short period. While it is also possible that this rise of small mode organics was the result of organics being involved in the initial growth, the comparatively high background level of traffic ultrafine organics during this event and the relatively noisy signals of m/z 44, a mass spectral marker of oxygenated organic species (*50*), limited our ability to ascertain this point conclusively for this particular event.

A discernible increase of $NH_4^{+}{}_{33-60}$ was observed after 10:00 a.m., about 45 min after the rapid increase of $SO_4^{2-}{}_{33-60}$ (Figure 5a). This delay suggests that the growth of the new particles during this stage was dominated by condensation of H_2SO_4 without enough NH_3 to neutralize the growing particles. The later uptake of NH_3 by the particles occurred as it became available (e.g., from traffic emissions) (*51*). However, this observed lag does not rule out the involvement of NH_3 in the nucleation mechanism since the amount of NH_3 needed for nucleating a particle is at least 3 orders of magnitude smaller than that needed for neutralizing H_2SO_4 in the ultrafine particles measured by the AMS. It is estimated that given the high concentrations of SO_2, and therefore H_2SO_4 production in sunny days, $NH_3-H_2SO_4-H_2O$ ternary nucleation is favored in Pittsburgh for as low as 10 ppt NH_3 (*52*).

Org_{33-60} resumed a second rise at ~11:15 a.m., when $NO_3^{-}{}_{33-60}$ also began to increase (Figure 5a). The increases seem to be a result of condensation of photochemical products onto ultrafine particles. Because of its very low concentration compared to the other three species (e.g., ~1% of the M_{33-60}) and the comparatively later rise of $NO_3^{-}{}_{33-60}$, nitrate seemed to have played a minor role in growing the new particles.

As mentioned earlier in this section, the smallest particles measured by the AMS during nucleation events were not freshly formed but rather grew from the nucleation mode that was formed ~1−2 h before. We thus calculated the characteristic times of coagulation and condensation to compare the relative importance of these two mechanisms for the growth of the nuclei to the minimum size detectable by the AMS. According to our calculations, the growth of nucleation mode particles due to gaseous condensation was approximately an order of magnitude faster than that due to coagulation. The later would have required more than 10 h to grow the nucleation mode particles to the smallest size detectable by the AMS. Therefore, we are unable to derive the composition of original nuclei from these AMS measurements but rather identify the species that contributed to the condensational growth.

The mass fractions of each individual species in the 33−60 nm mode as a function of the total ($M_{33-60} = SO_4^{2-}{}_{33-60} + NO_3^{-}{}_{33-60} + NH_4^{+}{}_{33-60} + Org_{33-60}$) shows that before nucleation Org_{33-60} was the dominant species, accounting for ~90% of M_{33-60} (Figure 5b). $SO_4^{2-}{}_{33-60}$ quickly overtook Org_{33-60} after the nucleation started and became the major species (>50% in mass) in the ultrafine mode between 10:30 a.m. and 2:00 p.m. (Figure 5b). $NH_4^{+}{}_{33-60}$ also rose substantially during the same period. Afterward, the concentrations of sulfate and ammonium in the 33−60 nm mode gradually declined back to their pre-nucleation levels while Org_{33-60} kept rising and regained dominance (Figure 5b). There is evidence (see section 3.2.4) that the ultrafine organic aerosols present at high concentrations right before and after the nucleation was mainly generated from combustion processes (most likely traffic).

3.2.3. Particle Acidities. Particle acidity was examined based on the ratio of measured ammonium concentrations versus the amounts needed to fully neutralize the measured sulfate and nitrate. A value of one suggests that sulfate and nitrate might be fully neutralized by ammonium in the form of $(NH_4)_2SO_4$ and NH_4NO_3. A value close to zero suggests that the particles are predominately H_2SO_4. On the basis of this definition, ultrafine particles (D_{va} = 33−60 nm) appeared to be acidic during the initial stage of the nucleation and gradually became neutralized (Figure 6a). Very acidic particles seemed to exist between 9:00 and 12:00, consistent with the observation of an earlier and faster increase of $SO_4^{2-}{}_{33-60}$ as compared to $NH_4^{+}{}_{33-60}$ (Figures 5a and 6a). It is interesting that although the start of the increase of ultrafine ammonium occurred ~45 min later than that of sulfate, it took more than 2 h for the ultrafine particles to be fully neutralized. This observation reinforces the conclusion that NH_3 was present at very low concentrations during the initial stages of the new particle formation event. In contrast, the two larger modes, the intermediate mode (D_{va} = 100−200 nm) and the accumulation mode (D_{va} = 300−500 nm), appeared to be nearly neutralized throughout the whole event (Figure 6b,c), probably because they were aged.

3.2.4. Possible Role of Organic Vapors in Growth of Ultrafine Particles (D_{va} = 33−60 nm). Size distributions of four organic fragments (i.e., m/z 43, 44, 55, and 57) were measured. Usually, m/z 44 (most likely the CO_2^{+} ion fragment) is a good tracer for photochemically formed secondary organic aerosol (*48*, *50*), while m/z 57 ($C_4H_9^{+}$) is generally associated with primary organics from combustion sources (*38*, *42*, *44*, *50*). m/z 43 and 55 can be produced by both primary combustion aerosols ($C_3H_7^{+}$ and $C_4H_7^{+}$, respectively)

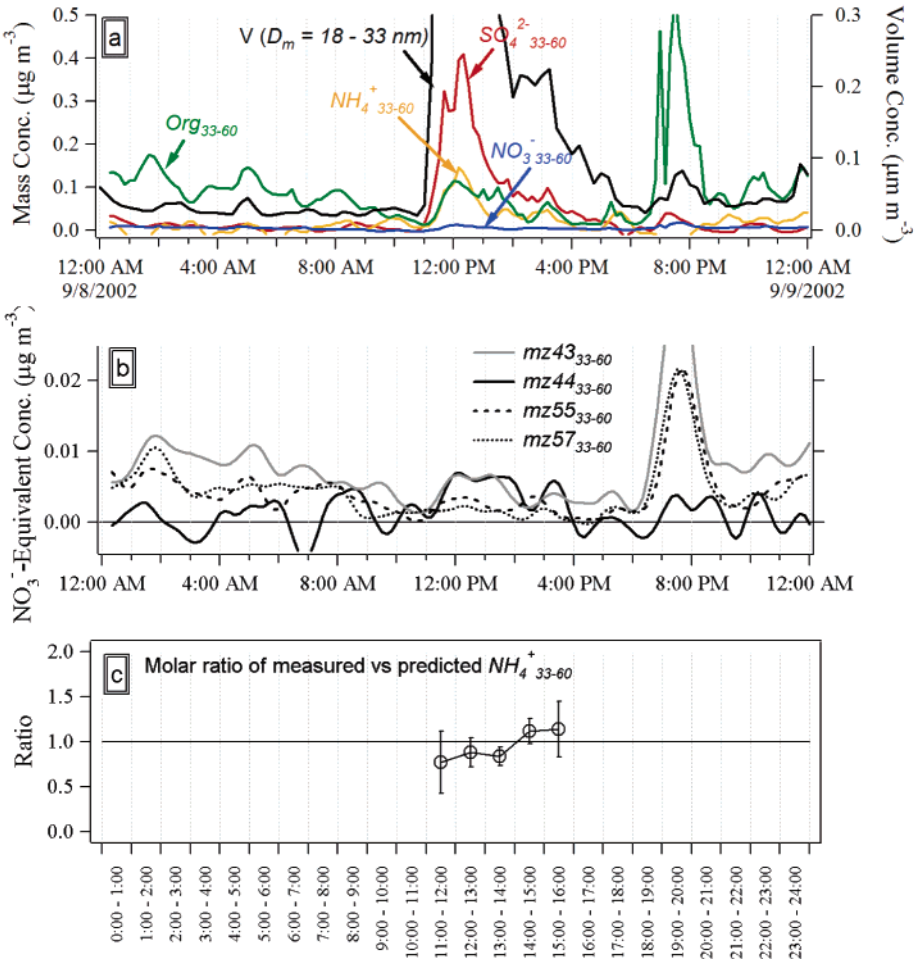

FIGURE 8. Variations of (a) concentrations of SO_4^{2-}, NH_4^+, NO_3^-, organics, and apparent particle volume: (b) NO_3^- equivalent mass concentrations of organic fragments (*m/z* 43, 44, 55, and 57); and (c) 1-h average of the mole ratio of measured NH_4^+ vs predicted NH_4^+ in the 33−60 nm (D_{va}) particles during September 8, 2002. See the caption of Figure 5 for other details.

and secondary photochemical aerosols ($C_2H_3O^+$ and $C_3H_3O^+$, respectively). *m/z* 43 seems to be produced in roughly equal fractions from primary and secondary organic aerosols; therefore, its time trend and size distributions most closely resemble those of the total organics. Indeed, we found that the mass ratio of *m/z* 43 to total organics was fairly constant throughout the whole campaign (*42*). *m/z* 55, on the other hand, seems to be produced more intensely from primary than from secondary organics (*48*). The time variations of these four fragments, in which *m/z* 55 and 57 peaked in the morning during rush hours while *m/z* 44 built up during the day when photochemistry is more intense, corroborate these qualitative associations (Figure 7a). A more in-depth discussion of the AMS organic fragments is given in separate papers (*42*, *50*).

A distinctive increase of *m/z* 44 in the 33−60 nm particles was observed at ~12:00 p.m., likely due to increased photochemical production of secondary organic aerosol (Figure 7a). The time series of $m/z\ 43_{33-60}$ tracked that of $m/z\ 44_{33-60}$ between 12:00 and ~5:00 p.m. but instead tracked those of $m/z\ 55_{33-60}$ and $m/z\ 57_{33-60}$ nicely before and after the nucleation event (Figure 7a). Because *m/z* 43 often correlated well with bulk particulate organics, not only in mass loading but also in size distribution (*42*), the synchronous increase of *m/z* 43 and 44 in the ultrafine mode between ~12:00 and 4:00 p.m. suggests that photochemically formed secondary organics contributed significantly to the growth of ultrafine particles during this period of time.

As shown in Figure 7, before the nucleation event *m/z* 55 and 57 were mainly in the ultrafine mode while *m/z* 44 was in the accumulation mode. These observations support our hypothesis that the Aitken mode organics prior to the nucleation were predominantly primary aerosols emitted from combustion processes. During stages I and II (8:10−12:05), the mass concentrations of ultrafine *m/z* 55 and 57 were generally decreasing (Figure 7d′,e′), because of atmospheric dilution and reduced traffic emissions compared to morning rush hours. The concentrations of ultrafine *m/z* 43 and 44, however, increased after stage I (Figure 7b′,c′), probably due to photochemical production of their parent organic compounds. The development of the size distributions of these four organic fragments during the last two stages (III and IV) were fairly similar—all grew into three modes that match those of the sulfate (Figures 7b′−e′ and 3d′), indicating either an extensive condensation of organic vapors during the later stages of the nucleation event or coagulation of the primary particles with the nucleation mode.

3.3. Evolution of Particle Chemistry during the Other Two Observed Nucleation Events. As mentioned in section 3.1, the general characteristics and meteorology of the other two nucleation days (September 8 and 9) resembled those of September 12. In addition, we found that the major traits of the growth dynamics of sulfate, ammonium, organics, and nitrate in the ultrafine mode (D_{va} = 33−60 nm) were similar among these three events as well. First of all, all of the ultrafine species increased significantly, although the absolute growth rates varied substantially from one event to another (Table 2). Such differences reflect variations in the intensity of the individual event (e.g., the increase rate of the number

concentration of the nucleation mode particles; Table 1). Second, sulfate and ammonium appeared to be the major contributors to the growth of ultrafine particles during all three events (Table 2), and interestingly, a rapid increase of $SO_4^{2-}{}_{33-60}$ always happened before that of $NH_4^+{}_{33-60}$, by 10−40 min. As a result, ultrafine particles were more acidic during the initial stages of the nucleation events and became more and more neutralized later on (Figures 6a and 8c). In addition, NO_3^- typically contributed very little (<3%) to the growth of ultrafine particles (Table 2).

The average rates and duration of the growth of ultrafine sulfate and ammonium varied considerably among these three nucleation events (Table 2). In comparison to the September 12 event (Figure 8), the September 8 nucleation event was characterized with a weaker burst of N_{10} but a much faster, and relatively short-lived, growth of $SO_4^{2-}{}_{33-60}$ and $NH_4^+{}_{33-60}$ (Tables 1 and 2; Figure 8). The exceptionally high ambient SO_2 concentration during the September 8 event (maximum = 156.4 ppb, vs maximum of 54.7 ppb on September 12) and comparatively fewer new particles might be responsible for the fast growth. It also appears that the spatial extent of the September 8 event was smaller than that of the September 12 and that more intense nucleation on September 8 took place upwind of our sampling site. Distinctive growth of the Org_{33-60} was observed during all three nucleation events (Table 2). Although the onset of the particle bursts varied by more than 2 h from one day to another (e.g., from 8:15 a.m. on September 12 to 10:30 a.m. on September 8; Table 1) significant increase in the mass of ultrafine organics (D_{va} = 33−60 nm) all started between 11:00 a.m. and 12:00 p.m. (Table 2). In addition, the observed growth of ultrafine organics appeared to be mainly attributed to the increases of $m/z\ 44_{33-60}$ and $m/z\ 43_{33-60}$ (e.g., Figures 7a and 8b), suggesting that secondary organic species played an important role in the growth of the new particles.

Acknowledgments

We thank Dr. Beth Wittig (CMU) for providing meteorological and gas phase data, Dr. Andrey Khlystov (CMU) for logistical assistance, Frank Drewnick (MPI) and James Allan (UMIST) for AMS data analysis software, and Dr. Owen Cooper (NOAA) for help with the HYSPLIT program. This research was conducted as part of the Pittsburgh Air Quality Study and was supported by the University of Colorado through startup funds for J.L.J., and by the U.S. Environmental Protection Agency under Contract R82806101.

Literature Cited

(1) Stanier, C.; Khlystov, A.; Pandis, S. *Aerosol Sci. Technol.* **2004**, *38*, 253−264.
(2) Kulmala, M.; Hameri, K.; Aalto, P. P.; Makela, J. M.; Pirjola, L.; Nilsson, E. D.; Buzorius, G.; Rannik, U.; Dal Maso, M.; Seidl, W.; Hoffman, T.; Janson, R.; Hansson, H. C.; Viisanen, Y.; Laaksonen, A.; O'Dowd, C. D. *Tellus Ser. B* **2001**, *53*, 324−343.
(3) Kulmala, M.; Toivonen, A.; Makela, J. M.; Laaksonen, A. *Tellus Ser. B* **1998**, *50*, 449−462.
(4) O'Dowd, C. D.; Geever, M.; Hill, M. K. *Geophys. Res. Lett.* **1998**, *25*, 1661−1664.
(5) O'Dowd, C. D.; Hameri, K.; Makela, J. M.; Pirjola, L.; Kulmala, M.; Jennings, S. G.; Berresheim, H.; Hansson, H. C.; de Leeuw, G.; Kunz, G. J.; Allen, A. G.; Hewitt, C. N.; Jackson, A.; Viisanen, Y.; Hoffmann, T. *J. Geophys. Res.-Atmos.* **2002**, *107*, 8108.
(6) O'Dowd, C. D.; Jimenez, J. L.; Bahreini, R.; Flagan, R. C.; Seinfeld, J. H.; Hameri, K.; Pirjola, L.; Kulmala, M.; Jennings, S. G.; Hoffmann, T. *Nature* **2002**, *417*, 632−636.
(7) Wiedensohler, A.; Wehner, B.; Birmili, W. *J. Aerosol Med.* **2002**, *15*, 237−243.
(8) Eisele, F. L.; McMurry, P. H. *Philos. Trans. R. Soc. London, Ser. B* **1997**, *352*, 191−200.
(9) Weber, R. J.; McMurry, P. H.; Mauldin, R. L.; Tanner, D. J.; Eisele, F. L.; Clarke, A. D.; Kapustin, V. N. *Geophys. Res. Lett.* **1999**, *26*, 307−310.
(10) Weber, R. J.; McMurry, P. H.; Eisele, F. L.; Tanner, D. J. *J. Atmos. Sci* **1995**, *52*, 2242−2257.
(11) Weber, R. J.; Marti, J. J.; McMurry, P. H.; Eisele, F. L.; Tanner, D. J.; Jefferson, A. *J. Geophys. Res.-Atmos.* **1997**, *102*, 4375−4385.
(12) Pirjola, L.; Laaksonen, A.; Aalo, P.; Kulmala, M. *J. Geophys. Res.-Atmos.* **1998**, *103*, 8309−8321.
(13) Weber, R. J.; Orsini, D.; Wang, B.; Scheuer, E.; Talbot, R. W.; Dibb, J. E.; Seid, G. K.; DeBell, L.; Mauldin, R. L.; Kosciuch, E.; Cantrell, C.; Eisele, F. *J. Geophys. Res.-Atmos.* **2003**, *108*, 8357.
(14) Woo, K. S.; Chen, D. R.; Pui, D. Y. H.; McMurry, P. H. *Aerosol Sci. Technol.* **2001**, *34*, 75−87.
(15) Hameri, K.; Kulmala, M.; Aalto, P.; Leszczynski, K.; Visuri, R.; Hamekoski, K. *Atmos. Res.* **1996**, *41*, 281−298.
(16) Harrison, R. M.; Grenfell, J. L.; Savage, N.; Allen, A.; Chemitshaw, K. C.; Penkett, S.; Hewitt, C. N.; Davison, B. *J. Geophys. Res.-Atmos.* **2000**, *105*, 17819−17832.
(17) Shi, J. P.; Evans, D. E.; Khan, A. A.; Harrison, R. M. *Atmos. Environ.* **2001**, *35*, 1193−1202.
(18) Alam, A.; Shi, J. P.; Harrison, R. M. *J. Geophys. Res.-Atmos.* **2003**, *108*, 4093.
(19) Dunn, M. J.; Jiménez, J.-L.; Baumgardner, D.; Castro, T.; McMurry, P. H.; Smith, J. N. *Geophys. Res. Lett.* **2004**, *31*, L10102, doi: 10110.11029/12004GL019483.
(20) Obersdorster, G. In *Ultrafine Particles in the Atmosphere*; Brown, L. M., Collings, N., Harrison, R. M., Maynard, A. D., Maynard, R. L., Eds.; Imperial College Press: London, 2003.
(21) Donaldson, K.; Brown, D.; Clouter, A.; Duffin, R.; MacNee, W.; Renwick, L.; Tran, L.; Stone, V. *J. Aerosol Med.* **2002**, *15*, 213−220.
(22) Donaldson, K.; Li, X. Y.; Macnee, W. *J. Aerosol Sci.* **1998**, *29*, 553−560.
(23) Brown, L. M.; Collings, N.; Harrison, R. M.; Maynard, A. D.; Maynard, R. L. *Philos. Trans. R. Soc. London Ser. A* **2000**, *358*, 2563−2565.
(24) Li, N.; Sioutas, C.; Cho, A.; Schmitz, D.; Misra, C.; Sempf, J.; Wang, M. Y.; Oberley, T.; Froines, J.; Nel, A. *Environ. Health Perspect* **2003**, *111*, 455−460.
(25) Kulmala, M.; Pirjola, U.; Makela, J. M. *Nature* **2000**, *404*, 66−69.
(26) Adams, P. J.; Seinfeld, J. H. *Geophys. Res. Lett.* **2003**, *30*.
(27) Kulmala, M.; Korhonen, P.; Napari, I.; Karlsson, A.; Berresheim, H.; O'Dowd, C. D. *J. Geophys. Res.-Atmos.* **2002**, *107*, 8111.
(28) Lazaridis, M. *Atmos. Environ.* **2001**, *35*, 599−607.
(29) Zhang, K. M.; Wexler, A. S. *J. Geophys. Res.-Atmos.* **2002**, *107*, 4577.
(30) Kerminen, V. M. *J. Aerosol Sci* **1999**, *30*, 1069−1078.
(31) Kulmala, M.; Dal Maso, M.; Makela, J. M.; Pirjola, L.; Vakeva, M.; Aalto, P.; Miikkulainen, P.; Hameri, K.; O'Dowd, C. D. *Tellus Ser. B* **2001**, *53*, 479−490.
(32) Birmili, W.; Wiedensohler, A.; Heintzenberg, J.; Lehmann, K. *J. Geophys. Res.-Atmos.* **2001**, *106*, 32005−32018.
(33) McMurry, P. H.; Woo, K. S.; Weber, R.; Chen, D. R.; Pui, D. Y. H. *Philos. Trans. R. Soc. London Ser. A* **2000**, *358*, 2625−2642.
(34) Smith, J. N.; Moore, K. F.; McMurry, P. H.; Eisele, F. L. *Aerosol Sci. Technol.* **2004**, *38*, 100−110.
(35) Voisin, D.; Smith, J. N.; Sakurai, H.; McMurry, P. H.; Eisele, F. L. *Aerosol Sci. Technol.* **2003**, *37*, 471−475.
(36) Smith, J. N.; Moore, K. F.; Eisele, F. L.; Ghimire, A. K.; Sakurai, H.; McMurry, P. H. In *Proceedings of the ACS Nanotechnology and the Environment Symposium* (submitted for publication).
(37) Jayne, J. T.; Leard, D. C.; Zhang, X.; Davidovits, P.; Smith, K. A.; Kolb, C. E.; Worsnop, D. R. *Aerosol Sci. Technol.* **2000**, *33*, 49−70.
(38) Jimenez, J. L.; Jayne, J. T.; Shi, Q.; Kolb, C. E.; Worsnop, D. R.; Yourshaw, I.; Seinfeld, J. H.; Flagan, R. C.; Zhang, X.; Smith, K. A.; Morris, J. W.; Davidovits, P. *J. Geophys. Res.-Atmos.* **2003**, *108*, 8425, doi: 8410:1029/2001JD001213.
(39) Jimenez, J. L.; Bahreini, R.; Cocker, D. R.; Zhuang, H.; Varutbangkul, V.; Flagan, R. C.; Seinfeld, J. H.; O'Dowd, C.; Hoffmann, T. *J. Geophys. Res.-Atmos.* **2003**, *108*, 4318, doi: 4310.1029/2002JD002452.
(40) Wittig, A. E.; Anderson, N.; Khlystov, A. Y.; Pandis, S. N.; Davidson, C.; Robinson, A. L. *Atmos. Environ.* **2004**, *38*, 3107−3125.
(41) Allan, J. D.; Jimenez, J. L.; Williams, P. I.; Alfarra, M. R.; Bower, K. N.; Jayne, J. T.; Coe, H.; Worsnop, D. R. *J. Geophys. Res.-Atmos.* **2003**, *108*, 4090, doi: 4010.1029/2002JD002358.
(42) Zhang, Q.; Canagaratna, M. C.; Jayne, J. T.; Worsnop, D. R.; Jimenez, J. *J. Geophys. Res.-Atmos.* (in press).
(43) Allan, J. D.; Coe, H.; Bower, K. N.; Alfarra, M. R.; Delia, A. E.; Jimenez, J. L.; Middlebrook, A. M.; Drewnick, F.; Onasch, T. B.;

Canagaratna, M. R.; Jayne, J. T.; Worsnop, D. R. *J. Aerosol Sci.* **2004**, *35*, 909−922, doi: 910.1016/j.jaerosci.2004.l002.1007.
(44) Canagaratna, M. R.; Jayne, J. T.; Ghertner, D. A.; Herndon, S.; Shi, Q.; Jimenez, J. L.; Silva, P. J.; Williams, P.; Lanni, T.; Drewnick, F.; Demerjian, K. L.; Kolb, C. E.; Worsnop, D. R. *Aerosol Sci. Technol.* **2004**, *38*, 555−573, 510.1080/02786820490465504.
(45) Pirjola, L.; Kulmala, M.; Wilck, M.; Bischoff, A.; Stratmann, F.; Otto, E. *J. Aerosol Sci*. **1999**, *30*, 1079−1094.
(46) Park, S. H.; Lee, K. W.; Otto, E.; Fissan, H. *J. Aerosol Sci.* **1999**, *30*, 3−16.
(47) Baron, P. A.; Willeke, K. *Aerosol Measurement*: *Principles, Techniques, and Applications*; Wiley-Interscience: New York, 2001.
(48) Alfarra, M. R.; Coe, H.; Allan, J. D.; Bower, K. N.; Boudries, H.; Canagaratna, M. R.; Jimenez, J. L.; Jayne, J. T.; Garforth, A.; Li, S.-M.; Worsnop, D. R. *Atmos. Environ.* (in press).
(49) Drewnick, F.; Schwab, J. J.; Jayne, J. T.; Canagaratna, M.; Worsnop, D. R.; Demerjian, K. L. *Aerosol Sci. Technol.* **2004**, *38*, 92−103.
(50) Zhang, Q.; Alfarra, M. R.; Worsnop, D. R.; Allan, J. D.; Coe, H.; Canagaratna, M. R.; Jimenez, J. *Environ. Sci. Technol.* (manuscript in progress).
(51) Fraser, M. P.; Cass, G. R. *Environ. Sci. Technol.* **1998**, *32*, 1053−1057.
(52) Napari, I.; Noppel, M.; Vehkamaki, H.; Kulmala, M. *J. Geophys. Res.-Atmos.* **2002**, *107*, 4381.

Received for review December 17, 2003. Revised manuscript received June 22, 2004. Accepted June 24, 2004.

ES035417U